

Performance of a CsI(Tl) calorimeter in an experiment with stopped K^+ 's

Yu.G. Kudenko*

Institute for Nuclear Research RAS, 117312 Moscow, Russia
For the KEK-E246 Collaboration

Abstract

The performance of the photon detector constructed for the search of T-violation in the decay $K^+ \rightarrow \pi^0 \mu^+ \nu$ is presented. The specific features of this detector consisting of 768 CsI(Tl) crystals with PIN photodiode readout for high precision measurement of T-odd correlations in decays of positive kaons are considered.

1 Introduction

The main goal of experiment E246 at the KEK 12 GeV proton synchrotron is a search for T-violating transverse muon polarization (P_T) in the decay $K^+ \rightarrow \pi^0 \mu^+ \nu$ ($K_{\mu 3}$) with a sensitivity of about $\Delta P_T \sim 10^{-3}$. The Standard Model predictions for P_T is less than 10^{-7} [1, 2] and a contribution from the final state interactions was found to be below the 10^{-5} level [3]. So, this experiment is able to search for additional or alternative sources of CP-violation postulated in various extensions to the Standard Model. In particular it is sensitive to the CP-violation in the multi Higgs doublet models, the leptoquark models and supersymmetric models with/without R-parity violation, where P_T can reach the measurable level of $10^{-4} - 10^{-2}$ [4].

The E246 detector was commissioned in 1996 and accumulated data for about 6 years. First results with a new limit on P_T were published in [6]. In this experiment, the $K_{\mu 3}$ decay is identified by detecting the π^0 as well as the μ^+ from the decay. The layout of the E246 set-up is shown in Fig. 1. A 660 MeV/c kaon beam is slowed down in a BeO degrader and stopped in an active target, made of 256 5×5 mm² scintillating fibers. The energy and direction of the π^0 from the $K_{\mu 3}$ decay are measured by a segmented CsI(Tl) photon detector installed in the central region of the

*email: kudenko@wocup.inr.troitsk.ru

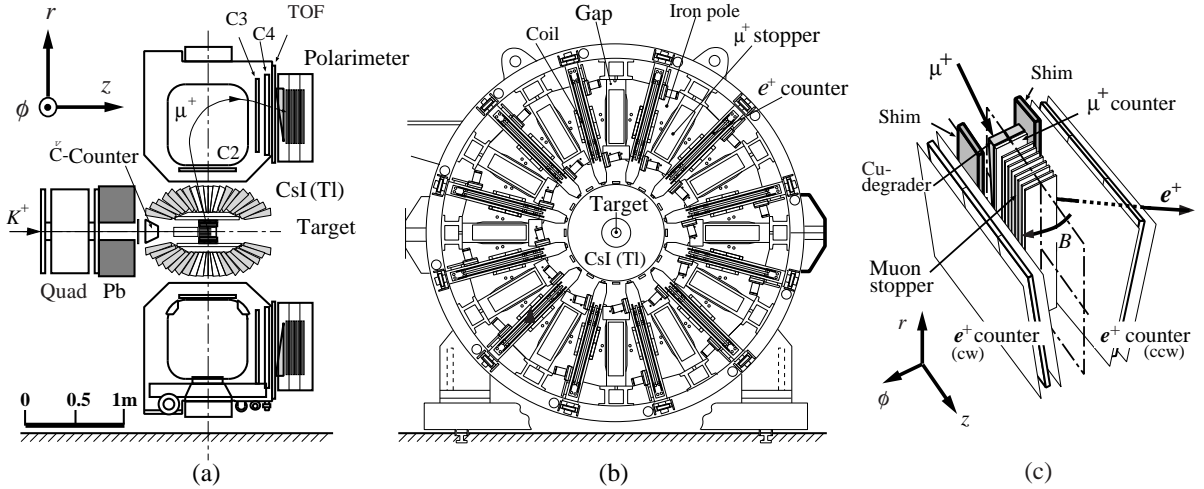


Figure 1: Experimental setup; (a) side view, (b) front view, and (c) one sector of the polarimeter.

toroidal magnet. A muon from the $K_{\mu 3}$ decay at rest is momentum-analyzed by one of the 12 magnet gaps of the superconducting toroidal spectrometer using tracking performed by the stopping target, a scintillating ring hodoscope [5] surrounding the target, and three MWPCs. The muon exiting the spectrometer is stopped in a polarimeter in which the decay positron asymmetry A_T is measured in order to obtain P_T . The polarimeter consists of 12 azimuthally arranged Al stoppers, aligned with the magnet gaps, with a scintillator counter system located between the stoppers. A positron from the decay of $\mu^+ \rightarrow e^+ \nu \nu$ tends to be emitted in the same direction as the muon spin, and is detected by these plastic scintillator counters. In this detector A_T appears as a difference in the counting rate between clockwise (cw) and counter-clockwise (ccw) emitted positrons. By summing the cw (N_{cw}) and ccw (N_{ccw}) positron counts over all 12 sectors, P_T is derived from

$$P_T = \frac{1}{\alpha f} \cdot \frac{N_{cw} - N_{ccw}}{N_{cw} + N_{ccw}}, \quad (1)$$

where α is the analyzing power of the polarimeter and f is an attenuation factor which reflects the fact that the decay plane of the $K_{\mu 3}$ event determined from the μ^+ and π^0 momenta is not parallel to the median plane of the gap in which the muon momentum is measured.

The photon detector plays a crucial role in this experiment for suppression of systematic errors. Using complete reconstruction of the $K_{\mu 3}$ kinematics we separate

these events into two classes: events with the pion moving along the kaon beam (forward direction) and those where the pion moves in the backward direction. The sign of P_T for the forward-going π^0 events is opposite to that for backward-going π^0 events. This allows us to apply a double ratio between the forward- and backward-going π^0 events cancelling out most instrumental sources of false polarization, which are likely to be independent of the π^0 direction. This method is a unique feature of E246 experiment, and is a key factor for effective suppression of most systematic errors.

2 Overall description of the calorimeter

The photon detector consists of 768 CsI(Tl) crystals each with a PIN photodiode readout. They form a barrel structure that covers about 75% of 4π with 12 symmetrically spaced holes for μ^+ s going into the magnetic spectrometer (Fig. 2).

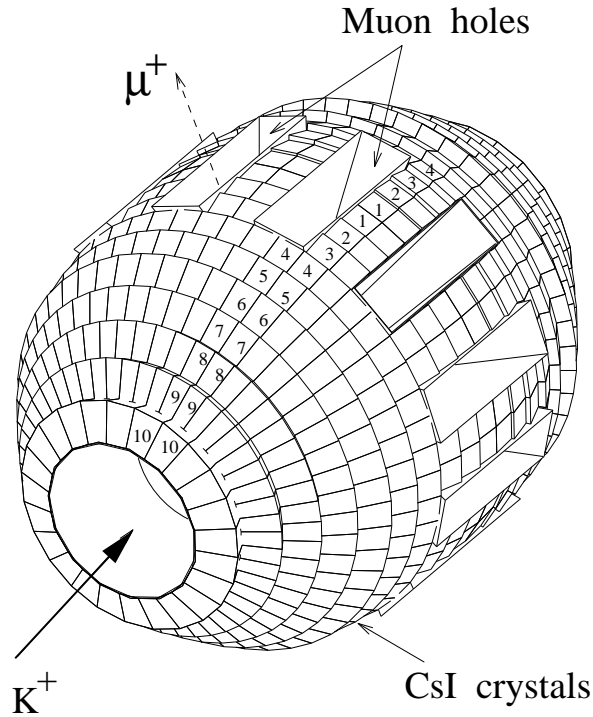


Figure 2: The photon detector.

The detector is capable detecting photons emerging from the target in the polar angle range from 15° to 165° and in 2π of the azimuthal angle except for the muon

holes. The optically isolated CsI modules point towards the center of the active target. An individual crystal covers 7.5° in both polar and azimuthal angles, except for 48 crystals near to the beam axis, where the azimuthal angle was doubled to 15° , and the muon hole region. The crystal length of 250 mm (13.5 r.l.) was chosen in order to leave about 4 cm of space available radially to mount a PIN-diode and preamplifier. The overall gain stability of the calorimeter is monitored by a Xe-lamp light pulser system with optical fibers which distribute the light from the lamp to the crystals.

To obtain uniform high light yield along the crystal, the crystal surfaces were treated to grade the reflectivity, and a Millipore white paper was chosen as a reflector (see for details Ref. [7]). As a result, for almost all modules the light yield of more than 8000 p.e./MeV and the average equivalent noise level (ENL) of about 63 keV were obtained, as shown in Fig. 3. The whole detector demonstrated a low level of

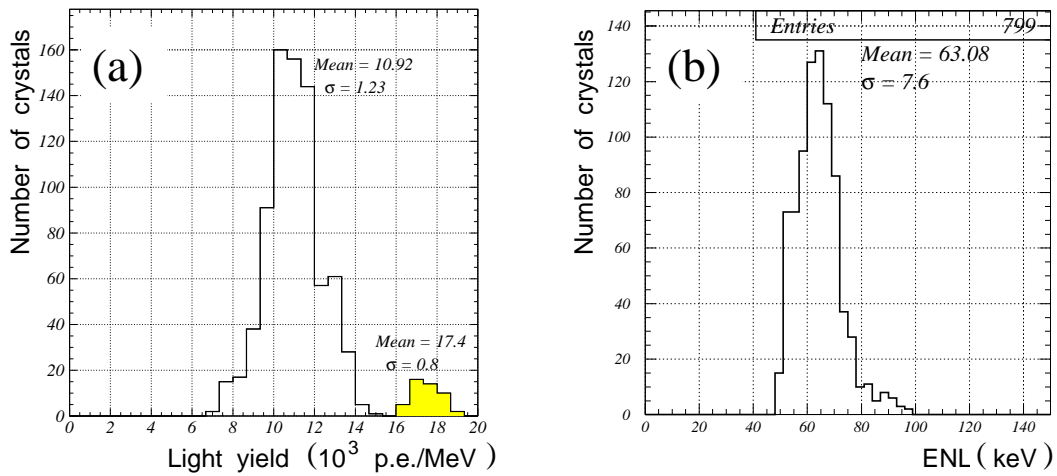


Figure 3: (a) Distribution of the light yield. The shadowed region of 16000–20000 p.e./MeV corresponds to the modules which have a PD with $28 \times 28 \text{ mm}^2$ sensitive area. (b) Distribution of the equivalent noise level.

coherent noise of about 11 keV (σ) per module, which has only a small effect on the energy resolution and signal-to-noise ratio of the detector. These parameters are the best among the large CsI(Tl) calorimeters which have been built in recent time [9].

To efficiently use the high light yield and low ENL of individual crystals, the electronics for the calorimeter was specially designed. The high counting rate environment in the calorimeter due to pion contamination in the beam was also taken into account in the design. The calorimeter electronics is schematically shown in Fig. 4 and described in detail in Ref. [10]. The main amplifier incorporates a shaping amplifier with fast restoration of the base level and a timing filter amplifier which

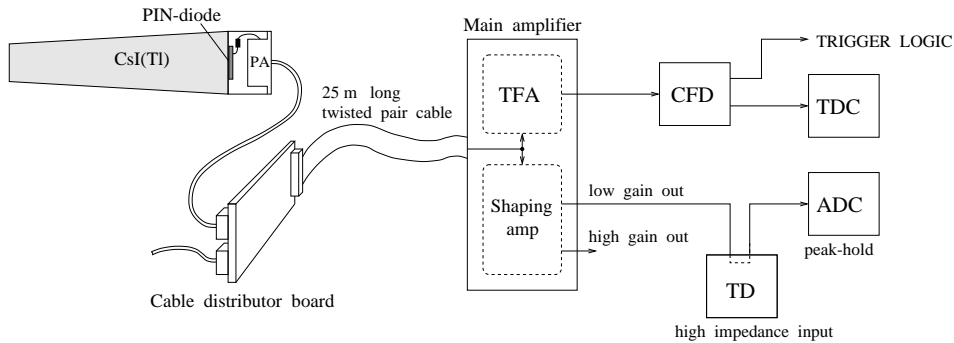


Figure 4: Electronics of a CsI module.

forms a timing signal for a subsequent discrimination by a constant fraction discriminator (CFD). The CsI timing signals from all CFD outputs are used in the second level trigger in coincidence with the first level fast trigger.

The detector stability is monitored by a Xe-lamp system. During the nearly 6 year period of operation none of the 768 photodiodes and only two preamplifiers failed. A light yield degradation of the CsI modules of about 12% was observed over this time.

3 Performance

3.1 In-beam calibration

The in-beam calibration of the detector was carried out using muons from the dominant decay mode $K^+ \rightarrow \mu^+ \nu$ of stopped kaons. These muons have a kinetic energy of 152.4 MeV and are stopped in the CsI crystals. The calibration runs, which were carried out every beam cycle, used a reduced beam intensity and a special trigger. It included the kaon identification with the Cherenkov detector, kaon stop in the target, and the presence of a signal in the CsI. In-flight kaon decays were avoided by introducing a 15-ns time delay. The events in which no energy was detected in the neighboring crystals were selected to obtain the individual gains of CsI modules. The kaon decay vertex was reconstructed from μ^+ tracking and muon energy losses in the target were corrected using the target fiber ADC information [11]. Using individual CsI calibration coefficients the decay $K^+ \rightarrow \pi^+ \pi^0$ is reconstructed. Fig. 5 shows the spectrum of the energy sum of two photon clusters from the decay $\pi^0 \rightarrow \gamma \gamma$. The peak value 235.7 MeV corresponds to about 96% of the $E_{\pi^0} = 245.6$ MeV, that is consistent with the result of Monte Carlo calculation for the cluster size of 5×5 crystals. The low energy tail is due to the shower leakage into the muon and beam holes, and through the rear sides of the crystals. The resolution σ_E/E obtained for the energy sum of two photons from $K_{\pi 2}$ decay is 5.2%. The energy resolution is better for clusters away from muon holes, as seen from Fig. 5(b). The

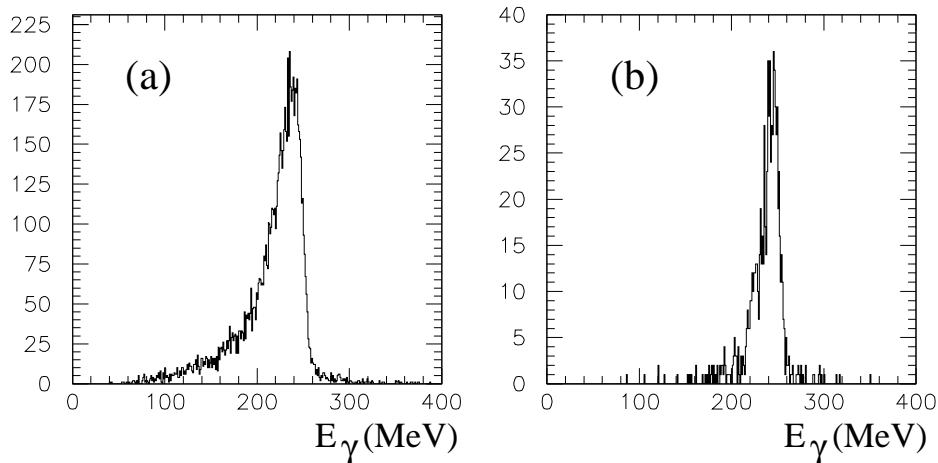


Figure 5: Energy sum of two 5×5 photon clusters from the $K_{\pi 2}$ decay. (a) All events with peak value $E_{\gamma\gamma} = 235.7$ MeV, $\sigma = 5.2\%$. The low energy tail is due to the shower leakage into muon and beam holes. (b) Photons are detected away from muon holes. $E_{\gamma\gamma} = 242.5$ MeV, $\sigma = 4.1\%$.

invariant mass resolution of the π^0 was 6.7% for whole detector and 5.6% for events with both photons detected away from muon holes.

3.2 Time resolution

Good time resolution is an important factor for reliable identification of photons and neutral pions from the decays of K^+ 's and for background suppression. The time resolution was determined in physics runs by measuring time difference between a muon signal from $K_{\mu 3}$ decay produced by one of the 12 fiducial plastic counters surrounding the target, and a CFD signal from a CsI module. Fig. 6 shows energy dependence of the obtained time resolution (σ) of the CsI crystals which are the centers of the gamma clusters. Time resolution of 3.5 ns at 100 MeV deteriorates to 16.8 ns in the low energy range of 10–20 MeV. For the $K_{\mu 3}$ photon energy range of 10–250 MeV the resolution $\sigma = 3.8$ nsec was obtained. To exploit the timing performance, all the CsI CFD outputs were added to the trigger logic as the OR strobe. A 150 ns discriminator pulse width was sufficient to accept nearly all good events, while reducing the recorded trigger rate by a factor of 2.

3.3 Counting rate

The slow decay time of CsI(Tl) crystals can lead to losses of detected events in a high intensity beam due to pile-up of the CsI pulses. The large contamination

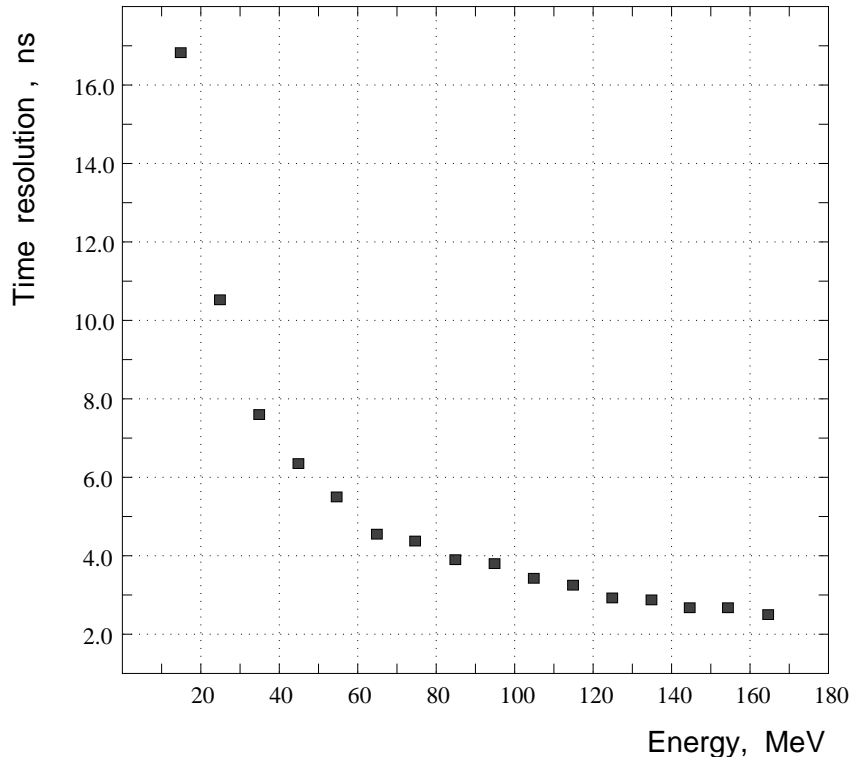


Figure 6: Time resolution as a function of the photon energy.

of pions in the beam ($\pi/K \geq 6$) and an asymmetrical pion halo were the main sources which dominated the counting rate in the calorimeter. The counting rate of a crystal depends on its position relative to the beam axis and was dramatically increased for the crystals closest to the beam, as seen in Fig. 7. Taking into account the distribution of the events over the solid angle, the average counting rate per crystal in the experiment was determined to be about 8 kHz. The tests of baseline stability at this counting rate using Xe-lamp events showed that about 5% of events were lost in physics runs due to pile up.

3.4 Detector alignment

The limited accuracy of the detector installation can make an asymmetry in the angular distribution between the median plane of the polarimeter and $K_{\mu 3}$ decay plane, the normal vector \vec{n} to which is defined as

$$\vec{n} = \frac{\vec{p}_{\pi^0} \times \vec{p}_{\mu^+}}{|\vec{p}_{\pi^0} \times \vec{p}_{\mu^+}|}. \quad (2)$$

Here \vec{p}_{π^0} and \vec{p}_{μ^+} are the momenta of the pion and muon, respectively. This angular asymmetry can give rise to contamination of the in-plane polarization and can generate a spurious T-odd effect due to the opposite direction of this polarization for

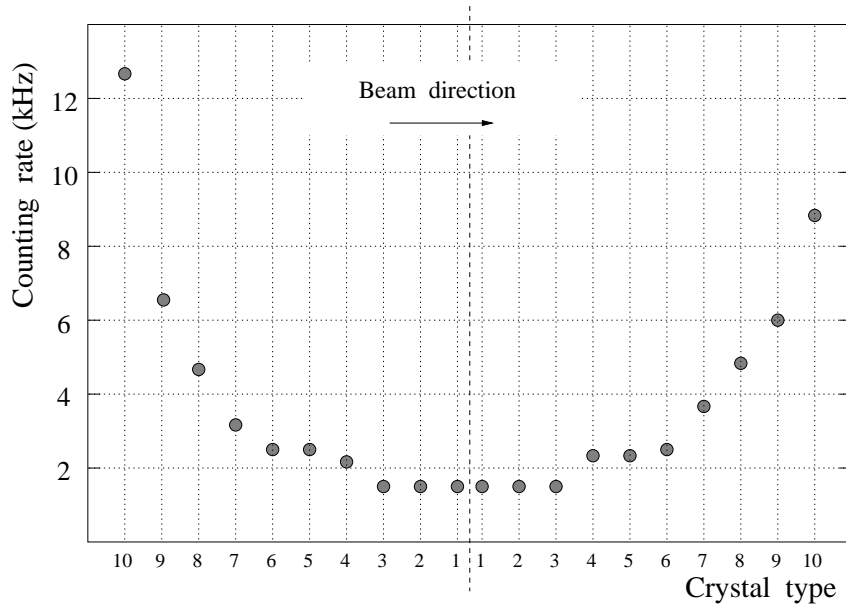


Figure 7: Counting rate in individual crystals. Position of each type of crystal in the calorimeter is shown in Fig. 2.

the forward- and backward-going pions. According to the Monte Carlo simulation, the residual value of the muon in-plane polarization in the polarimeter is 0.5–0.7 for both directions of the neutral pions. The measured angular distributions of $K_{\mu 3}$ decay plane rotations around the beam direction (z -axis) and radial direction (r -axis, perpendicular to the beam and lying in the median plane of a magnet sector, see Fig. 1(c)) are presented in Fig. 8. As one can see, the detector provides good angular symmetry, and possible spurious polarization caused by detector misalignment is $\leq 3.7 \times 10^{-4}$, i.e. much less than the expected statistical error.

3.5 Double ratio

To measure the power of the double ratio, the compensation of a large imitation asymmetry in the experimental kaon stopping distribution was studied for the good forward and backward $K_{\mu 3}$ events. The events accumulated in 1998 running cycle were selected, in the right-hand part of the target relative to the median plane in each magnet sector looking upstream the beam, as shown in Fig. 9. As a result, in each gap a spurious asymmetry of 2–6% appears, as seen in Fig. 10, and total asymmetry is $A_F = -2.90 \pm 0.21\%$ and $A_B = -2.65 \pm 0.21\%$ for forward and backward events, respectively. So, the double ratio

$$(A_F + A_B)/(A_F - A_B) \simeq 22 \quad (3)$$

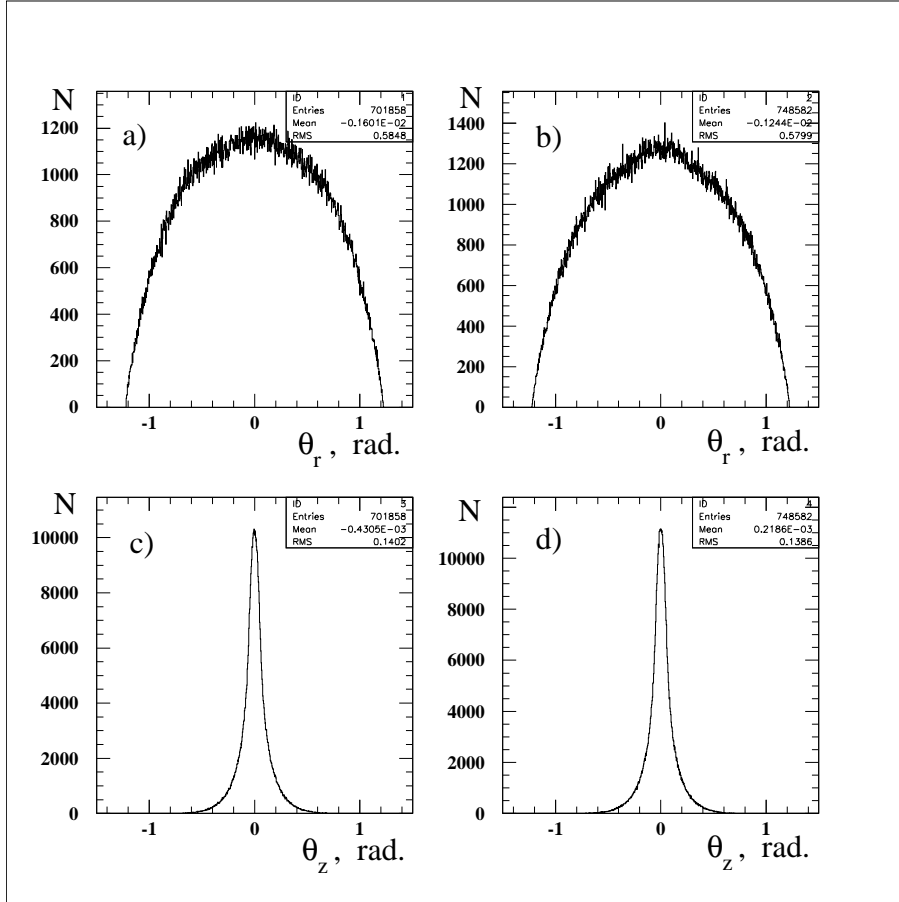


Figure 8: The $K_{\mu 3}$ decay plane rotation around r and z axes. (a) and (c) $K_{\mu 3}$ events with forward-going pions; (b) and (d) $K_{\mu 3}$ events with backward-going pions.

provides a large factor for cancellation of systematic errors in the asymmetry measurement. For different data sets this factor was determined to be in the range of 15-24.

4 Conclusion

The CsI(Tl) photon detector with PIN photodiode readout is being successfully used in the E246 experiment at KEK. The overall performance of the calorimeter was not degraded significantly after being in operation for 6 years. The CsI calorimeter provides good reconstruction of the π^0 parameters and seems to be a key instrument for reduction of systematic uncertainties in the polarization measurement down to the level of 10^{-3} that completely fulfills the requirements of the experiment.

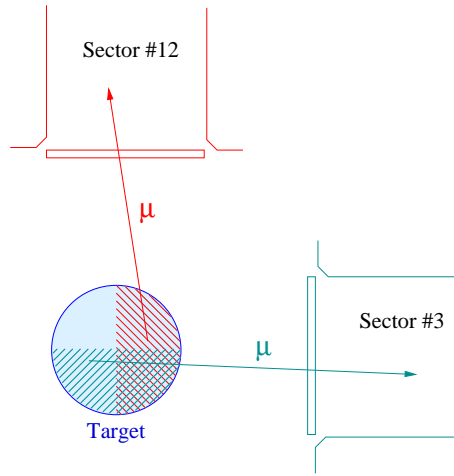


Figure 9: Schematic view of the events selection for study of the systematics compensation by double ratio

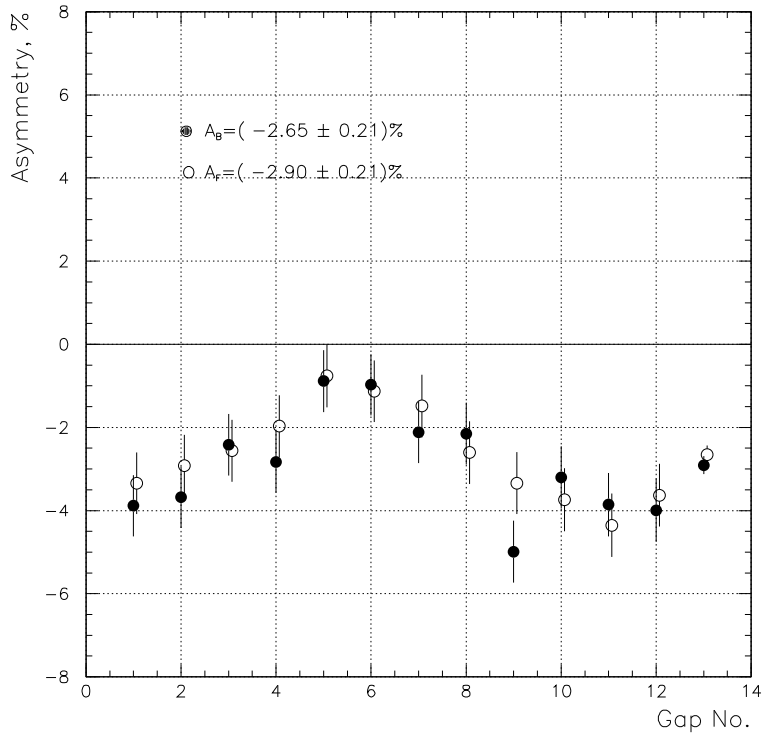


Figure 10: The illustration of the suppression of systematic errors using double ratio. The open (solid) circles represents $K_{\mu 3}$ events with forward (backward)-going pions selected as shown in Fig. 9. The values shown for Gap No.13 are sums of forward and backward asymmetries over all polarimeter sectors.

References

- [1] I.I. Bigi and A.I. Sanda, CP violation, Cambridge University Press, 2000.
- [2] E. Golowich and G. Valencia, Phys. Rev., **D40** (1989) 112.
- [3] A.R. Zhitnitskii, Yad. Fiz. **31** (1980) 1024.
V.P.Efrosinin et. al., Phys. Lett. **B493** (2000) 293, hep-ph/008199.
- [4] S. Weinberg, Phys. Rev. Lett. **37** (1976) 657.
G. Bélanger and C.Q. Geng, Phys. Rev. **D44** (1991) 2789.
G.-H. Wu and J.N. Ng, Phys. Lett. **B392** (1997) 93, hep-ph/9609314.
M. Fabbrichesi and F. Vissani, Phys. Rev. **D55** (1997) 5334, hep-ph/9611237.
- [5] A.P. Ivashkin et al., Nucl. Instr. Meth. **A394** (1997) 321.
- [6] M. Abe et al., Phys. Rev. Lett. **83** (1999) 4253.
- [7] M.P. Grigorev et. al., Instr. Exp. Tech. **39** (1996) 164 [Prib. Tekhn. Eksp. **N2** (1996) 18].
- [8] D.V. Dementyev et al., Nucl. Instr. Meth. **A440** (2000) 151.
- [9] Y. Kubota et al., Nucl. Instr. Meth. **A320** (1992) 66.
E. Aker et al., Nucl. Instr. Meth. **A321** (1992) 69.
B. Shwartz, “Crystal calorimeters”, talk at this Conference, <http://www.inp.nsk.su/events/confs/instr2002/day5.shtml>; K. Miyabayashi, “BELLE electromagnetic calorimeter”, *ibid*; B.Lewandowski, “Design and performance of the BaBar EM calorimeter”, *ibid*.
- [10] Yu.G. Kudenko, O.V. Mineev, J. Imazato, Nucl. Instr. Meth. **A411** (1998) 437.
- [11] M.M. Khabibullin et al., Instr. Exp. Tech. **43** (2000) 589 [Prib. Tekhn. Eksp. **N5** (2000) 9].